Geophys. J. Int. (2008) **174,** 659–671 doi: 10.1111/j.1365-246X.2008.03838.x

Seismic moment release during slab rupture beneath the Banda Sea

Mike Sandiford

School of Earth Sciences, University of Melbourne, Victoria 3010*, Australia. E-mail: mikes@unimelb.edu.au*

Accepted 2008 April 30. Received 2008 April 30; in original form 2007 August 15

SUMMARY

The highest intermediate depth moment release rates in Indonesia occur in the slab beneath the largely submerged segment of the Banda arc in the Banda Sea to the east of Roma, termed the Damar Zone. The most active, western-part of this zone is characterized by downdip extension, with moment release rates ($\sim 10^{18}$ Nm yr^{-1} per 50 km strike length) implying the slab is stretching at $\sim 10^{-14}$ s^{-1} consistent with near complete slab decoupling across the 100–200 km depth range. Differential vertical stretching along the length of the Damar Zone is consistent with a slab rupture front at ∼100–200 km depth beneath Roma propagating eastwards at ∼100 km Myr^{-1}. Complexities in the slab deformation field are revealed by a narrow zone of anomalous in-plane *P*-axis trends beneath Damar, where subhorizontal constriction suggests extreme stress concentrations ∼100 km ahead of the slab rupture front. Such stress concentrations may explain the anomalously deep ocean gateways in this region, in which case ongoing slab rupture may have played a key role in modulating the Indonesian throughflow in the Banda Sea over the last few million years.

Key words: Seismicity and tectonics; Subduction zone processes; Asia.

1 INTRODUCTION

The rupture of subducting slabs from the trailing surface plate that must inevitably accompany continent-arc 'collision' is a crucial process in the plate tectonic cycle (Davies & von Blackenburg 1995). Consequently, numerous studies have attempted to elucidate the mechanisms of slab rupture using constraints derived from seismic tomography (Spakman 1990), forward modelling (Yoshioka & Wortel 1995; Wong *et al.* 1997; Gerya *et al.* 2004) and geological observations (Meulen *et al.* 1998). Along with many others, these studies have progressed our understanding of slab rupture processes. However, they have yet to be adequately tested using constraints derived from the deformation field in actively rupturing slabs. A crucial set of data relevant to the instantaneous deformation field within deforming slabs is provided by focal mechanism solutions and moment tensor data. With a few notable exceptions (Nothard *et al*. 1996), past attempts to resolve the deformation field within slabs have been hampered by data limitations. However, the growth of the Harvard CMT catalogue now make it timely to reassess constraints on the deformation field in actively rupturing slab systems using moment release rates.

The Banda Sea in eastern Indonesia in one of the best locations to study active slab rupture (McCaffrey *et al.* 1985; McCaffrey 1989a, b; McCaffrey & Abers 1991). For well over 20 yr, it has been known that the ∼500 km long, now extinct, and actively uplifting (Merritts *et al.* 1998), section of the volcanic arc around Wetar and Alor, to the north of Timor, is underlain by a region of anomalously low intermediate depth seismicity compared to the volcanically active regions to either side (Figs 1 and 2, McCaffrey *et al.* 1985; McCaffrey 1989b; Das 2004). This study focuses on the nature of the deformation field at intermediate depths between Wetar and the zone of much more intense activity beneath the island of Damar, further east. It builds on the previous studies (Cardwell & Isacks 1978; McCaffrey *et al.* 1985; Das 2004; Milsom 2005) in utilizing the now greatly expanded set of data now available through the CMT catalogue. Seismic activity in this region has been previously investigated in several studies (Das 2004; Milsom 2005). Most notably, Das (2004) used a set of relocated events assembled in 1999 to describe the geometry of the slab system and reported relevant CMT solutions for the relocated events. As of 2007 October, the CMT catalogue comprised 226 intermediate depth (70–300 km) events between 127 and 131°E along the southern limb (south of 6°S) of the Banda slab in the vicinity of the island of Damar, providing a density data that allow much better resolution of deformation within the Banda slab, thereby leading to new insights into the mechanisms of slab rupture.

2 GEOLOGICAL AND GEOPHYSICAL SIGNALS OF SLAB DETACHMENT BENEATH THE BANDA SEA

Convergence between the Indo-Australian and Sunda plates is accommodated along both the Sunda and Banda arcs (Fig. 1). The Sunda arc comprises the active volcanic segment of the arc to the west of ∼122°E, where oceanic lithosphere of the Indo-Australian plate is being subducted. In the eastern part of the Sunda arc, from eastern Java to Sumbawa, earthquakes define a more or less continuous, steeply dipping, planar slab extending to transition zone

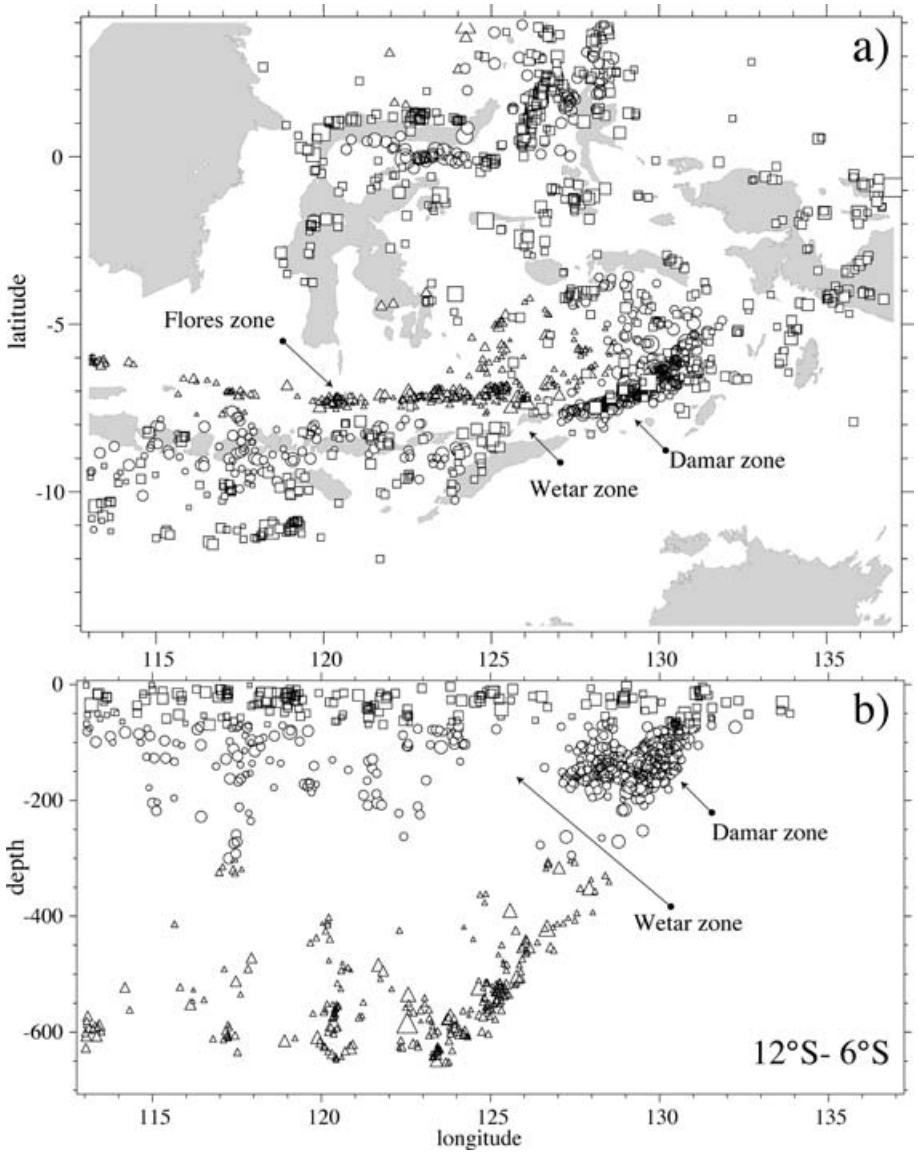

Figure 1. (a) Map showing composite relocated Indonesian (CIR) catalogue derived from Engdahl & Villaseñor (2002) and Schoffel & Das (1999). Triangles represent events greater than 300 km deep, circles events between 70 and 300 km and squares events less than 70 km. Symbol sizes are proportional to reported magnitudes (with a range from *M* 3.5–7.4). (b) Depth slice show event distribution for those events shown in panel (a) between 12°S and 6°S.

depths at ∼600 km (Fig. 2a, Schoffel & Das 1999; Das 2004). Tomographic imaging (Replumaz *et al*. 2004) shows the slab connects at subtransition zone depths to a large, seismically fast anomaly beneath the Sunda Plate. The Banda arc is distinguished because it juxtaposes Australian continental lithosphere against the forearc, representing one the best examples of active arc-continent collision on the modern earth. The geometry of the slab is well constrained by relocated earthquake data (e.g. Schoffel & Das 1999; Milsom 2001; Das 2004) and tomographic imaging (Widiyantoro & van der Hilst 1997). It comprises either (1) one continuous, but tightly folded, slab or (2) two or more distinct slabs of opposing vergence that meet at the surface near 132°E, 6°S (Milsom 2001). In the former case, the small radius of curvature (∼200 km) make it one of the most tightly folded slabs known, attributable to the unique geodynamic setting involving a combination of backarc spreading that opened the Banda Sea to the east at around 5 Ma and Pacific Plate motion that drives a westward motion of crustal blocks to the northeast of the Banda Sea, relative to Australia (McCaffrey 1989b).

In terms of volcanism, the southern limb of the Banda arc comprises three distinct segments: a ∼400 km long, volcanically active, segment to the west of Alor (here termed the Flores Zone); a ∼500 km long volcanically inactive segment including the islands of Alor, Atauro and Wetar to the north of Timor (termed the Wetar Zone); and sa ∼400 km long, volcanically active segment extending east and north from Damar around the Banda Sea to Ambon (termed the Damar Zone). Volcanism in the Wetar Zone ceased at about 3 Ma (Abbott & Chamalaun 1981), following collision between the Australian continental margin as marked by Pliocene tectonism on Timor (Audley-Charles 2004). Helium and strontium isotopes show systematic variations along the arc, and evidence significant contamination of magma source zones by continental crust, suggesting the leading edge of the Australian continental crust has been subducted

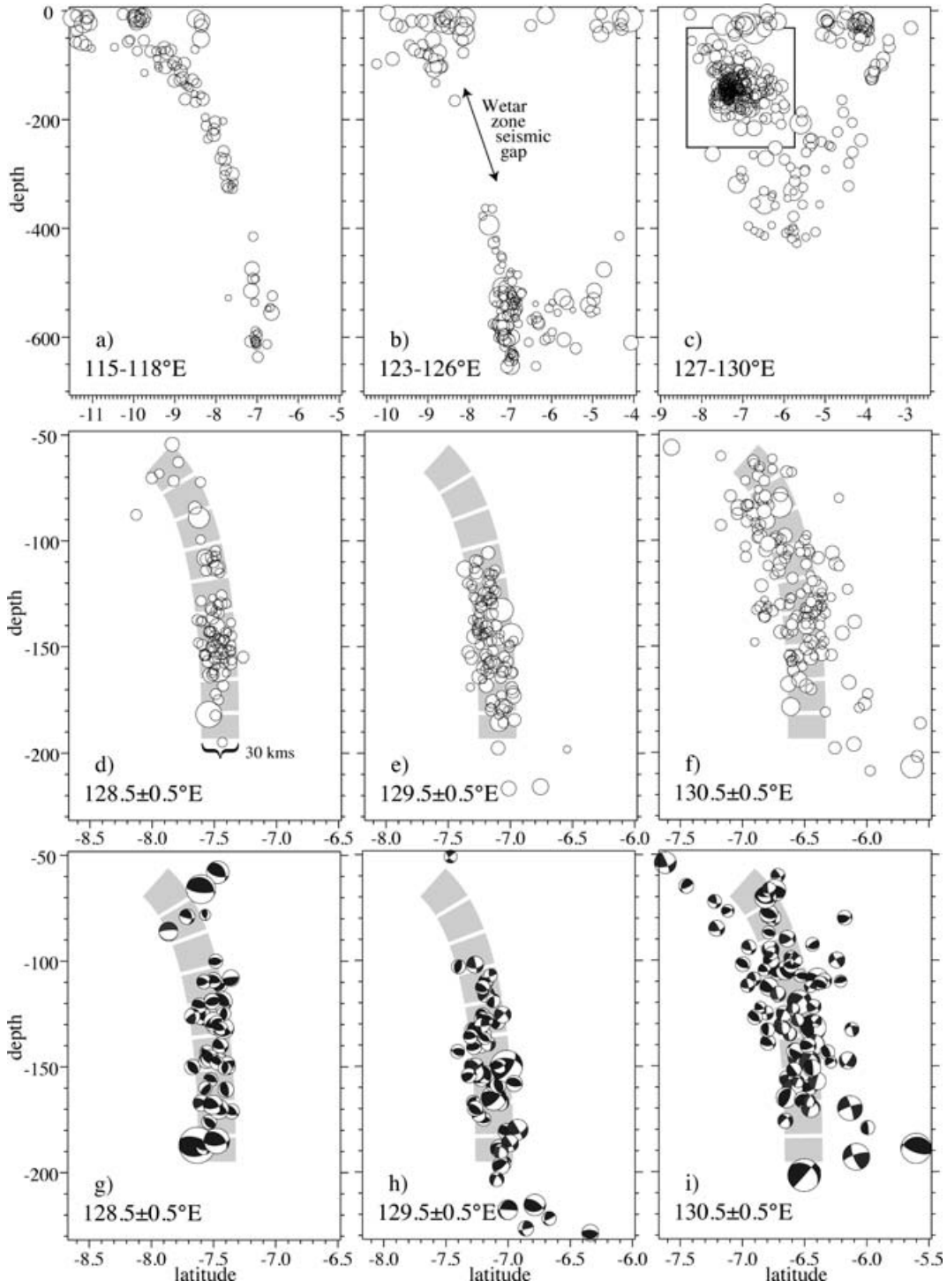

Figure 2. Panels (a–c): N–S sections using 3°-wide bins across segments of the Indonesian slabs using the CIR catalogue. (a) Section through the eastern Sunda slab. (b) Section through the islands of Timor, Wetar and Buru highlighting the intermediate depth seismic gap, and the distinct band of seismicity at depths greater than ∼400 km that connects the north dipping Benioff zone beneath Wetar with a south dipping Benioff zone beneath Buru on the northern side of the Banda Sea. (c) Section through the island of Damar and Seram in the eastern Banda sea, showing a diffuse band of seismicity connecting the southern and northern limbs of the Banda slab(s), highlighting the intense seismicity on the southern limb at depths 100–200 km. The boxed region is illustrated in detail in Panels (d–i). Panels (d–f) details of Damar Zone seismicity (CIR catalogue) in 1° wide boxes (∼110 km) projected onto a plane striking N022°W, perpendicular to the slab trace. The coordinates of the centres of the southern boundaries of the boxed regions are 128.5, 129.5 and 130.5°E and –8.75, –8.25 and –7.75°S, respectively. For scale the shaded region is 30 km wide, highlighting the widening of the zone of seismic activity to the east of Damar panel (f), near Leyeni. In the western part of the Damar Zone well-located earthquakes show a relatively narrow distribution consistent with seismogenic slab zone of <30 km wide. Panels (f–i) as for panels (d–f) but using the CMT solutions with focal mechanisms plotted as lower hemisphere projections.

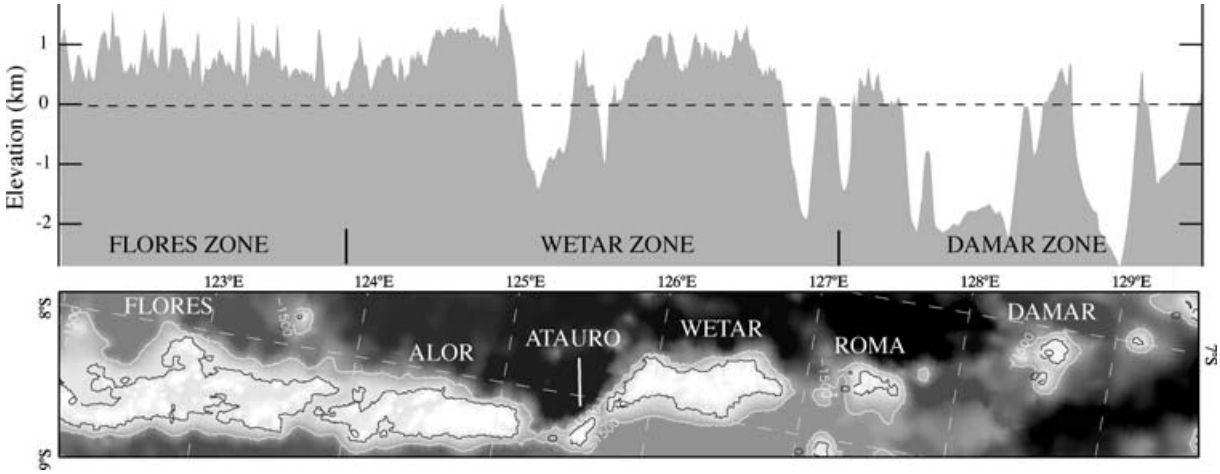

Figure 3. Topographic profile of highest points along the Banda Arc between ∼122°E and ∼130°E encompassing the mostly exposed Flores and Wetar Zones and largely submerged Damar Zone. The western limit of intermediate depth seismicity in the Damar Zone occurs at 127.4°E beneath Roma (see Figs 5 and 6).

to depths of at least 100 km during collision with the Banda arc (Hilton *et al.* 1992, 1993; Gasparon *et al.* 1994).

The boundary between the Wetar and Damar Zones, near the island of Roma at 127°30′E, is marked by a significant change in topography (Fig. 3). To the west the arc is mainly emergent with only narrow seaways separating the volcanic islands such as Wetar, Alor and Flores. To the east the arc is largely submerged with significant gateways as deep as ∼2 km. The Wetar Zone shows abundant

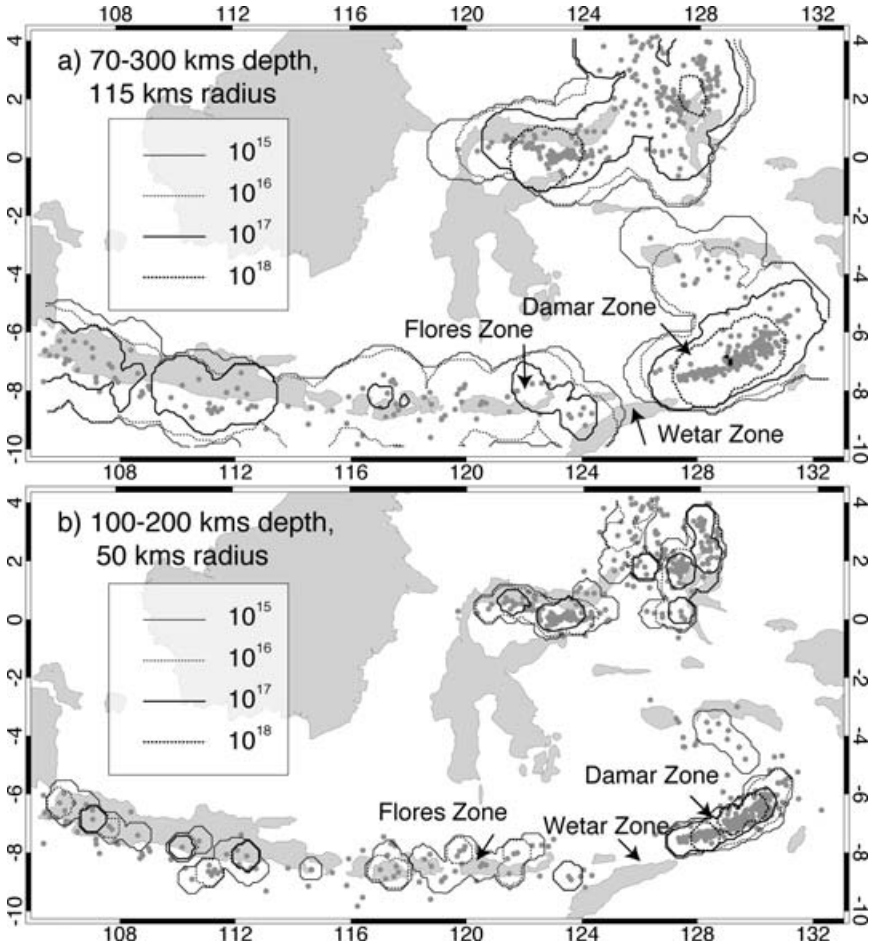

Figure 4. Summed scalar moments for the intermediate depth seismicity in the Indonesian region (contours in Nm yr^{-1}). (a) depth range 70–300 km summed for cylindrical volumes of surface radius = 115 km, (b) depth range 100–200 km computed for cylindrical volumes of surface radius of 50 km. Note that the intermediate depth seismic moment release rate of the Damar Zone is—one to two orders of magnitude higher than elsewhere in the Sunda and Banda arcs, while the seismic moment release rate of the Wetar Zone is the lowest in Sunda–Banda arc system.

evidence for emergence in the form of elevated Quaternary terraces, now hundreds of metres above sea level over a broad zone extending from Sumba in the west through to the eastern tip of Timor Leste (Merritts *et al.* 1998). Uplift rates are estimated at 0.5 mm yr^{-1} on Sumba (Pirazzoli *et al*. 1991) and Atauro (Chappell & Veeh 1978) and 1–1.2 mm yr^{-1} on Alor (Hantoro *et al.* 1994). Similar uplift rates are indicated for large uplifted, but essentially undeformed, coral terrace platforms in the eastern part of Timor Leste. Variations in uplift rate of almost an order of magnitude, from 0.2 to 1.5 mm yr^{-1}, have been reported from the islands of Serau and Rote, respectively (Merritts *et al*. 1998) and indicate that lithospheric deformation must play an important role in promoting uplift. However, the long wavelength uplift of about 0.5 mm yr^{-1} extending some 400 km from Alor through Atauro to the eastern end of Timor Leste is arguably a response to sublithospheric processes that may have direct bearing on the nature of processes operating in and around the slab beneath (see later discussion). Little is known of the bathymetric evolution of the largely submerged Damar Zone, which plays a crucial role in providing the principal gateway for the Indonesian throughflow, connecting the Pacific and Indian Oceans.

The notion that the Banda Slab has been partially ruptured from the surface plate in the vicinity of Timor is further informed by GPS and geological studies. Genrich *et al.* (1996) showed that both Timor and parts of the extinct section of the volcanic arc to its north are now effectively 'welded' to the Australian plate. The implication is that convergence between the Australian and Sunda Plates is now largely accommodated on the northern (or backarc) side of the extinct arc segment along the Wetar thrust. Shallow-depth seismic activity to the north of Flores and Wetar is significantly higher than along the Timor trench, confirming the notion that plate convergence is no longer kinematically connected to the subducted slab in a simple way. Slab rupture is likely to have commenced at ∼3 Ma when volcanism in the now extinct part of the arc ceased (Abbott & Chamalaun 1981; Audley-Charles 2004; Elburg *et al.* 2004). Published tomographic imaging (e.g. Widiyantoro & van der Hilst 1997) has not yet clearly resolved upper mantle structure beneath Wetar at the level required to elucidate details of slab structure associated with variations in seismic activity.

3 SEISMIC CHARACTER OF THE SOUTHERN BANDA SEA

In this paper several earthquake catalogues are used characterize the seismicity in the southern part of Banda Sea (south of 6°S). First, relocated events from the Centennial catalogue (Engdahl & Villaseñor 2002) have been combined with a catalogue of relocated Indonesian events assembled by (Schoffel & Das 1999). This composite catalogue of Indonesian relocated events (CIR) comprises a total of 1019 well-located events for the region between 12°–6°S and 113–137°E and provides for the best available constraint on the spatial distribution of Banda slab events (Figs 1 and 2). Second, some 747 focal mechanism solutions from the CMT catalogue, up to

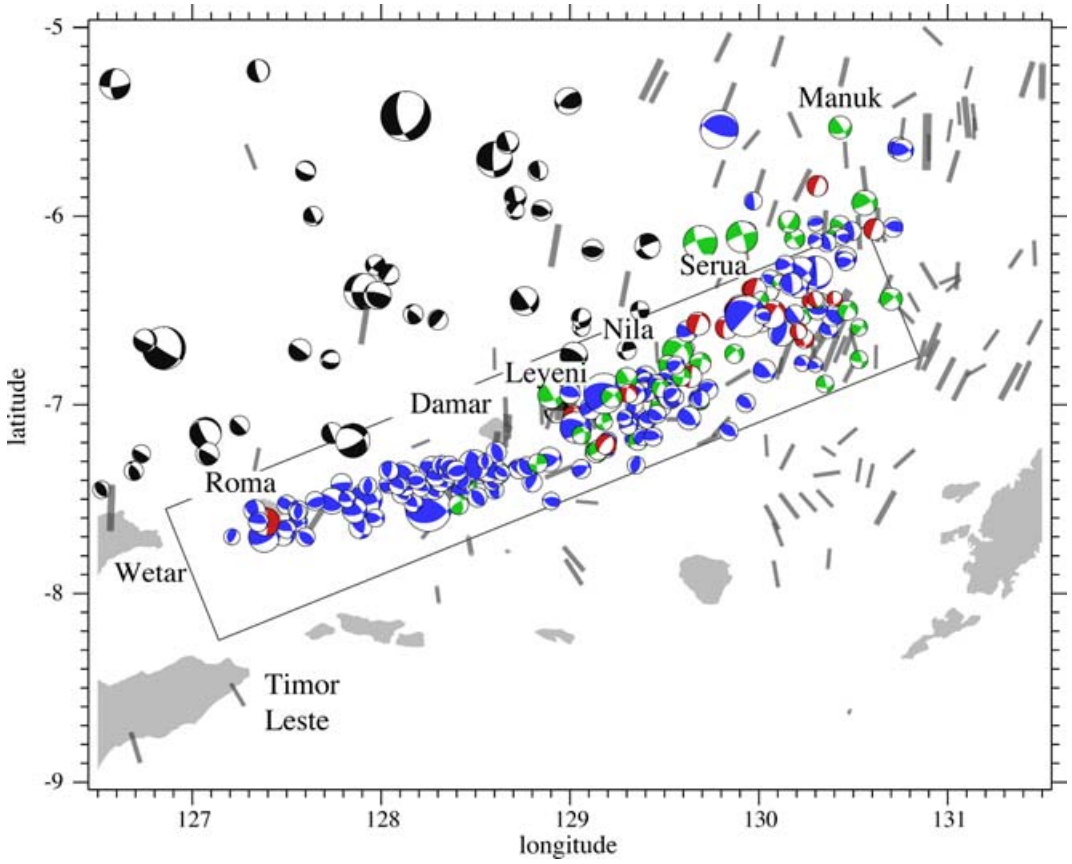

Figure 5. Map view for selected CMT focal mechanisms for the Damar Zone. Solutions in the depth range 95–205 km are colour coded by mechanism (red – normal fault, green – strike-slip and blue – reverse). Solutions with depths >205 km are shown in black. *P*-axis projections are shown for events with depths shallower than 95 km. The box shows the region analysed in Fig. 8, corresponding to the seismogenic slab in the depth range 100–200 km. The dashed segments within the box demarcate the individual selections used in the analysis shown in Fig. 8. (Colours in the online version only.)

and including 2007 October, for the same region are used to explore the deformation field within the Banda slab.

In accord with the findings of several previous studies (McCaffrey 1989a; Schoffel & Das 1999; Das 2004; Milsom 2005), both the CIR and CMT catalogues show that the Wetar Zone is characterized by a distinct gap in intermediate depth seismicity compared to the volcanically active regions on either side (Figs 1 and 2), and especially the Damar Zone to the east. At depths greater than ∼300 km, more or less continuous seismicity extends across the three zones with CMT solutions dominated by down dip compression typical of deep subduction earthquakes. The Damar Zone is by far the most seismically active portion of the Banda slab at intermediate depths (Fig. 4). Despite comprising only ∼15 per cent by arc-length, it accounts for ∼60 per cent of the eastern Sunda and Banda arc intermediate level events in the CMT catalogue. Intermediate depth volumetric scalar moment release rates obtained by summation of CMT events are more than an order of magnitude greater than in any other portion of the Banda or Sunda arc (Fig. 3). The Damar Zone includes the ∼M_w 8.3 1963 event (depth ∼100 km deep, epicentre 6.8°E, 129.58°E; Osada & Abe 1981), one of the largest intermediate known depth events recorded, as well as the ∼M_w 8.5 great Banda Sea earthquake of 1938 (depth ∼60 km, epicentre 5.06°S, 131.60°E), the ninth largest event of the 20th Century (Genrich *et al.* 1996; Kanamori 1997; Okal & Reymond 2003). In the last 50 yr, the Damar Zone has experienced six M_w 7+ events, making it one of the most active intermediate depth earthquake zones on the planet. The CMT catalogue includes 305 events in the Damar Zone including five M_w 7+ events, but does not include either of the M_w 8+ events referred to above (Figs 5 and 6). To the west of 129°30′E, intermediate depth seismicity is dominated by reverse fault mechanisms, reflecting downdip tension, with both catalogues showing the seismic activity is confined to a narrow zone ∼30 km in across-strike width, trending 068°E (Fig. 2). East of 129°30′E, intermediate depth activity is characterized by a mix of reverse, strike-slip and normal mechanisms distributed over a zone at least 80 km in across-strike width (Fig. 2f).

Within the Damar Zone the azimuth of principal axes of the moment tensors (*P*, *T*) show spatial variation allowing subdivision into distinct 'domains' (Figs 6–8). At shallow depths (<70 km) *P*-axes tend to be aligned at about 10–20°E broadly paralleling the Australian plate velocity (see Das 2004), consistent with stress regimes being dictated by plate boundary interactions. At intermediate depths, the *P*-axis alignment relative to the slab trend changes along the slab. As noted originally by Cardwell & Isacks (1978), east of ∼130.5°E, *P*-axes tend to be aligned in the plane of the slab. Between 130.5°E and 128.9°E, *P*-axes trend NNW, at a

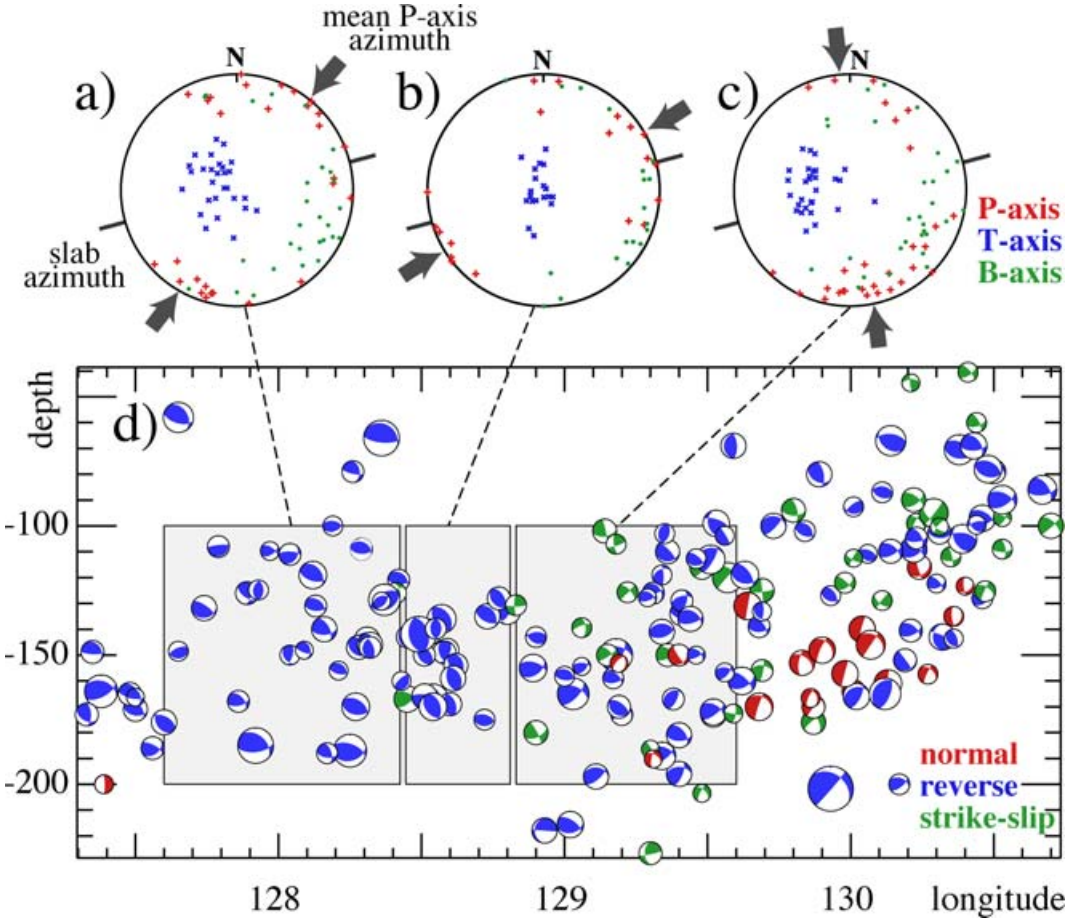

Figure 6. Depth slice showing CMT focal mechanism solutions for the southern limb of the Banda slab seismicity in the depth range 35–250 km. Note that only events from within the boxed region in Fig. 5 are used, and that the focal mechanisms are shown as lower hemisphere projections colour coded by mechanism (red – normal fault, green – strike-slip and blue – reverse). Stereographic nets show *P*-, *T*- and *B*-axes orientations for reverse mechanisms from each of the three boxed regions. And highlight the anomalous nature of the intermediate depth seismicity beneath the island of Damar at 128.5°E, where the *P*-axes are aligned more-or-less parallel to the trend of the slab (∼068°E). This contrasts the more 'typical' slab character of *P*-axes aligned at a high angle to the slab trend. (Colours in the online version only.)

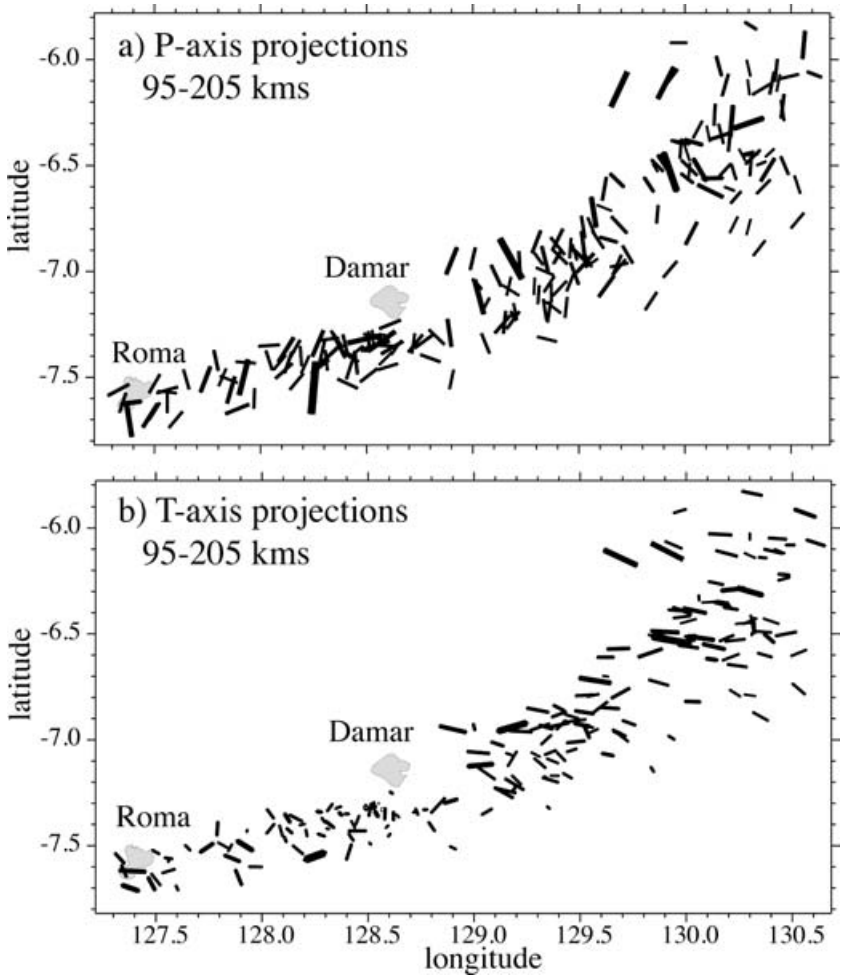

Figure 7. *P*-axis (a) and *T*-axis (b) projections for the southern limb of the Banda slab in the vicinity of Damar for the depth range 95–205 km. The size of the indicators are scaled for magnitude, as reflected by variations in the projected width of indicators (most of the variation in the projected length relates to variations in the plunge of the axes, as indicated by the mainly steeply plunging *T*-axes and shallow, slab-parallel *P*-axes near Damar).

high angle to the slab. In a narrow zone centred just south of Damar, *P*-axes are aligned within the plane of the slab. West of ∼128.2°E, the *P*-axes are aligned at a moderate angle to the slab trend more or less parallel to the shallower seismicity. The zone of slab parallel *P*-axes near Damar is characterized by a general steepening of *T*-axes that define a tight cluster with a median plunge of about 80°, implying that horizontal, in-plane slab shortening is accompanied by downdip stretching.

4 THE DAMAR ZONE DEFORMATION FIELD

The intense intermediate depth seismic activity in the Damar Zone demands that the slab is failing internally, suggesting that it may be the site of active slab rupture ahead of a slab window opening from the west. The plausibility of this model can be tested with reference to the seismic deformation field within the slab. This section uses moment tensor data from the CMT catalogue to quantify the deformation field using approaches adapted from previous studies (e.g. Nothard *et al*. 1996).

The principal components of the summed seismic moment release rate tensor for Damar Zone intermediate depth seismicity are summarized in Table 1 and shown in Figs 9 and 10 in terms of the six tensor components M_{rr}, M_{tt}, M_{pp}, M_{rt}, M_{rp} and M_{tp}. The summation

$$\bar{M}_{ij} = \sum_{k=1}^{N} M_{ij}^{k},$$

where M_{ij}^{k} is the ijth moment component of the kth earthquake, is taken over vertical cylinders of radius 25 km between 95 and 205 km depth. r, t and p refer to vertical (up), north and east directions, respectively: directions that are well aligned with respect to the principal moment axes as revealed by orientation of *P* and *T*-axes as shown in Figs 6(a–c). The mean moment release rates in this depth range, normalized to a slab volume equivalent to 50 km long by 100 km deep, with a seismogenic width of ∼30 km, are shown in Table 1.

Catalogue moment release rates are invariably biased by the location of the rare, large events, with frequency comparable to catalogue duration (see Figs 9a–c). The long-term spatial pattern of moment release is therefore better informed by using a 'reduced' catalogue including only events that have recurrence intervals that are significantly shorter than the catalogue record. Figs 9(d–i) and 10 show the reduced-moment release obtained by excluding the three largest CMT events (with $M_{\mathrm{w}} > 6.65$ or scalar moments greater than about 10^{19} Mm). Positive $\bar{M}_{rr}$ show that the Damar Zone slab is extending vertically along its entire length (Fig. 9d) while negative $\bar{M}_{tt}$

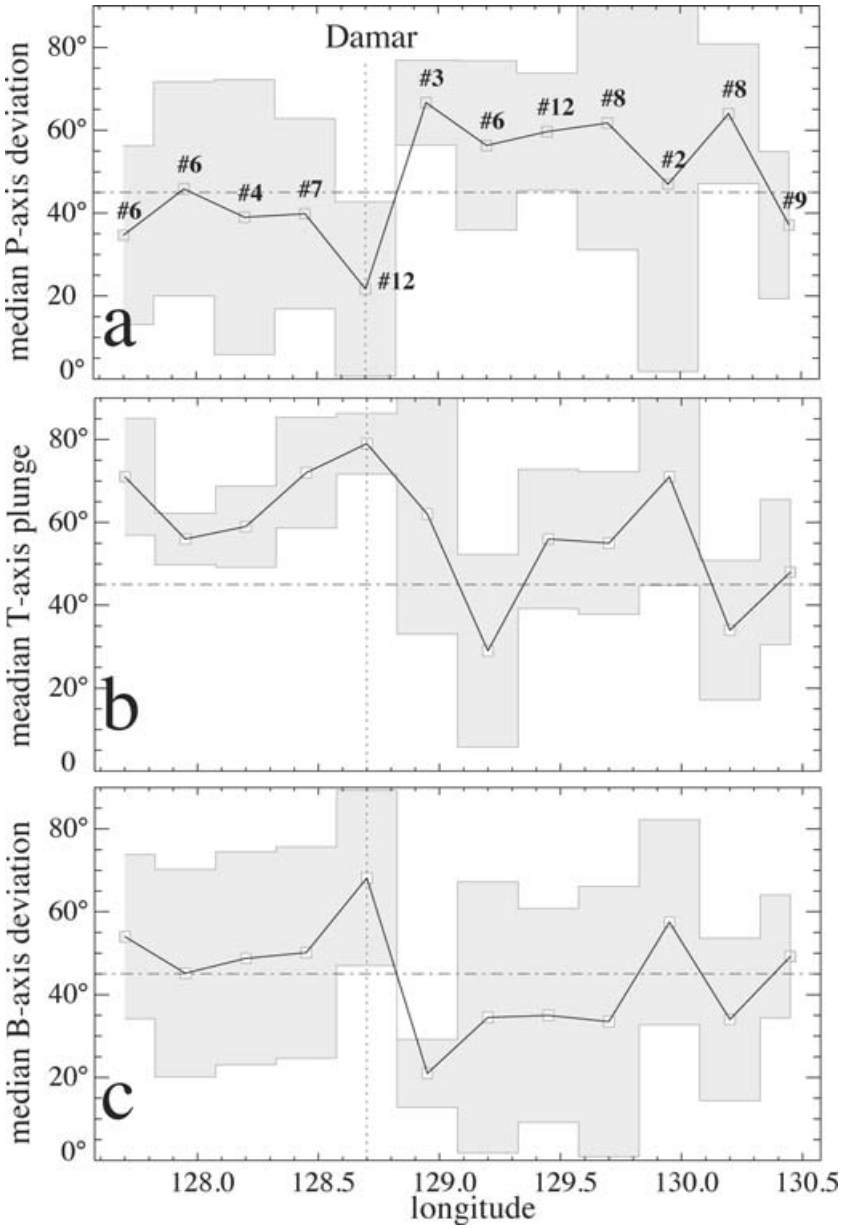

Figure 8. Characteristics of intermediate depth (95–205 km), CMT focal mechanism principal axes (*P*, *T*, *B*) for the Damar Zone. Panel (a): deviation of median *P*-axis trend from the 068°E (i.e. mean trend of the slab in the western Damar Zone). Panel (b): plunge of median *T*-axis. Panel (c): deviation of median *B*-axis trends from 068°E. The shaded zone shows ±1 *SD*. The number of mechanisms in each selected region are prefaced with a #.

Table 1. Summary of intermediate depth (100–200 km) seismic moment release rate and strain rate for the Damar Zone. Moment release rates are normalized to a slab segment 50 km long with a seismogenic width of ∼30 km. *r*, *t* and *p* refer to vertical (up), north and east directions, respectively. Positive values imply extension.

	rr	*tt*	*pp*	*rt*	*rp*	*tp*
$\bar{M}_{ij}$ (mm yr^{-1})	9.3×10^{17}	-9.6×10^{17}	3.5×10^{16}	-2.9×10^{16}	7.1×10^{17}	-9.4×10^{16}
ε_{ij}(s^{-1})	2.8×10^{-15}	-2.9×10^{-15}	1.1×10^{-16}	-8.6×10^{-17}	2.1×10^{-15}	-2.8×10^{-16}

show that it is thinning across the extent of the slab (Figs 9e). The reduced $\bar{M}_{rr}$ values are about typically three to five times higher in the western sector (west of 129°40′E) than in the eastern sector, implying differential vertical stretching along the slab (Fig. 10a). The sign of $\bar{M}_{pp}$ varies along the zone (Fig. 9f) with positive values showing that it is mostly extending along its length except in of the region near Damar, where negative $\bar{M}_{pp}$ reflect the in-plane shortening, as is indicated by the characteristic alignment of *P*-axes in the plane of the slab. Here, negative $\bar{M}_{pp}$ and $\bar{M}_{tt}$ imply the slab is undergoing horizontal constriction, with the associated maxima in $\bar{M}_{rr}$ implying vertical stretching at faster rates than any other part of the slab. In the segment to the west of the Damar constriction, absolute $\bar{M}_{pp}$ imply deformation approximates plane strain, while further east deformation involves mild flattening.

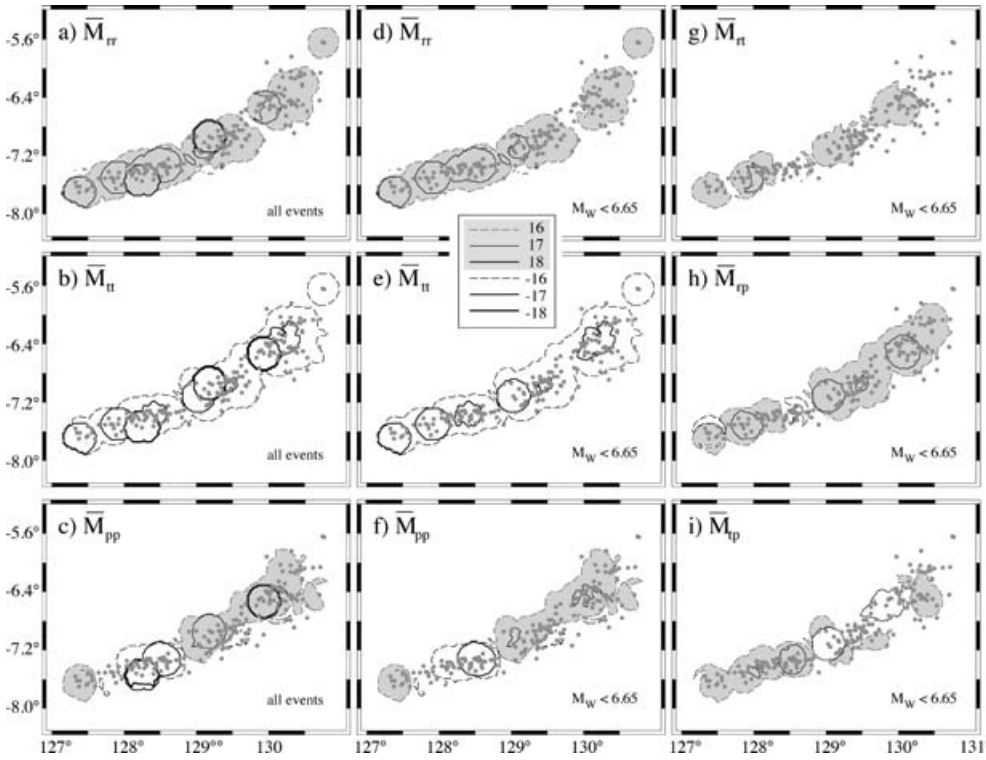

Figure 9. Summed components of the seismic moment tensor for intermediate depth seismicity in the Damar Zone (contours in units of log10 Nm yr^{-1}). *r*, *t* and *p* refer to vertical (up), north and east directions, respectively. Positive values are shown by shaded regions. Moments are summed over vertical cylindrical volumes with radius 25 km extending from 95 to 205 km depth. Figs (a–c) show summation over all events, while panels (d–i) show reduced moment summation for events with scalar moments less than 10^{23} Nm. See text for discussion.

Estimates of the seismogenic deformation rates can be derived from seismic moment release rates following Kostrov (1974):

$$\dot{\varepsilon}_{ij} = \frac{1}{2\mu v t}\bar{M}_{ij},$$

where μ is the shear modulus (3.5×10^{10} Nm^{-2}), v is the relevant volume over which seismic moments of the individual earthquakes are summed and t is the time interval of relevance. The mean value of $\bar{M}_{rr} \sim 10^{18}$ Nm yr^{-1} in the depth range 100–200 km, when normalized to a 50 km long by 30 km wide slab segment, corresponds to mean vertical stretching rate of $\sim 2.8 \times 10^{-15}$ s^{-1}. The reduced moment release profile in Fig. 10(a) suggests that maximum stretching rates are several times the mean for the fastest deforming zone between 127 and 128.7°E near Damar. Moreover, several factors suggest that the total seismogenic strain rates are likely to be both higher, and show more along strike variation, than indicated by the profiles of reduced moment release shown in Fig. 10.

First, because the very large events that dominate long-term moment release have recurrence intervals much longer than the duration of seismic records, they are typically not adequately represented in existing catalogues. Missing large events will result in catalogue-based moment release estimates to underestimate long-term moment release rates. That much higher moment events than recorded in the CMT catalogue have occurred is evidenced by the historical record of two M_w 8+ events in the 20th century, with the 1963 M_w 8.3 event occurring in the depth range 100–200 km relevant to the discussion here. However, the notional increase in moment up to some arbitrary magnitude M_{max} can be estimated assuming these events follow some statistical recurrence relation. For Guttenberg–Richter statistics the up-scaling factor is (e.g. Johnston *et al.* 1994):

$$M_o' \approx 10^{(c-b)(M_{max}-M_{obs})},$$

where M_{obs} is the largest catalogue event used in determining the moment, M_{max} is the maximum expected magnitude for earthquakes in the region of interest, b is the recurrence parameter (typically 1 for Guttenberg–Richter statistics) and c is a conversion factor of 1.5 relating moment magnitude scale to seismic moment (Hanks & Kanamori 1979). For a b-value of 1, increasing M_{max} from 7.4, the largest event in the CMT database, to 8.3, in order to incorporate the largest known historical event, equates to an increase of M_o' ~2.8. Because the extent to which large magnitude events ($M_w > \sim 7.5$) obey the Guttenberg–Richter scaling relations is unknown, the moment release rate estimate using this approach is clearly subject to significant uncertainty. Nevertheless, it does highlight the point that summation of CMT catalogue moments is likely to underestimate the long-term moment release rate by several factors.

Second, summed moment release rates are sensitive to the assumed width of the seismically active zone. The seismogenic slab has been assumed to be ~30 km wide, consistent with the observed distribution of both CIR- and CMT-catalogue events in the western end of the Damar slab (Fig. 2) as well as in other subduction zones such as Tonga (Nothard *et al.* 1996). However, other workers have suggested that slab seismicity may be confined to zones as little as 15 km wide (Houston 1993). Given uncertainties in earthquake locations this is certainly possible for the western part of the Damar Zone, implying that volumes associated with moment release may have been overestimated and associated strain rates underestimated. However, it is also clear that within the Damar slab the seismogenic

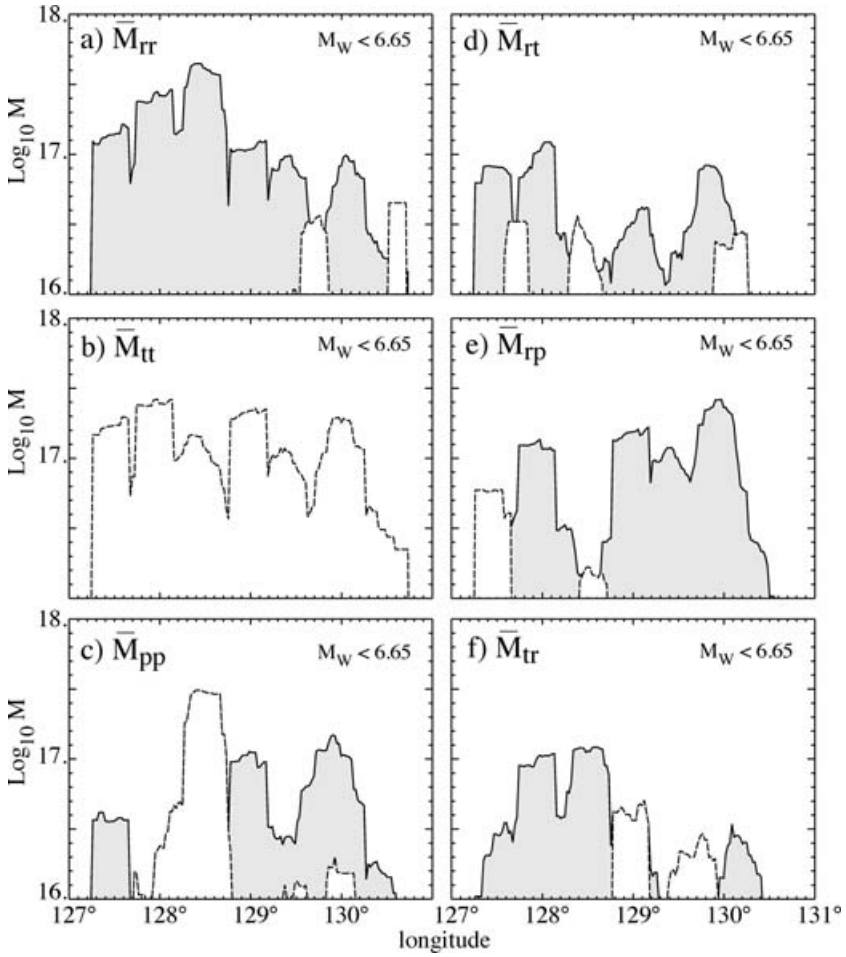

Figure 10. Longitudinal profiles of intermediate-depth, reduced moment release (log10 Nm yr^{-1}) along the Damar Zone (see Fig. 9 caption for details). Solid lines with grey shades for +ve summed moments and dashed line for –ve summed moments. Reduced moment release rates are used to understand the spatial pattern of moment release. As discussed in the text moments can be 'up-scaled' to obtained estimates for any assumed maximum magnitude event. For example, upscaling the reduced moments to $M_{\max} = 7.4$ (the largest Damar Zone event in the CMT catalogue), is obtained with a factor of 2.4, leading to a maximum $\bar{M}_{rr}$ value of 1.2×10^{18} Nm yr^{-1} and to $M_{\max} = 8.3$ (the largest intermediate depth Damar Zone event) with a factor of 6.7 with $\bar{M}_{rr}$ of 3.4×10^{18} Nm yr^{-1}.

zone broadens considerably to the west, and must be significantly wider than 30 km east of 130°E (Fig. 2f). One implication of this is that the gradient in the volumetric vertical moment release rate along the Damar slab must be significantly more marked than shown in Fig. 10(a).

Finally, we currently have no meaningful way of assessing the relative contributions of seismic and aseismic deformation within a deforming slab. However, by analogy with continental realms, where satellite based methods show that aseismic strain accumulation tends to exceed the seismically released strain, it is probable that a considerable portion of the strain in the deforming slab is accruing aseismically.

These factors caution that seismogenically determined moment-release and strain rates are highly uncertain. However, they mostly suggest that the estimates shown in Fig. 10 are conservative, implying that the mean vertical stretching rate due to seismic activity in the slab can be assumed to be at least 3×10^{-15} s^{-1}. In the region of greatest volumetric moment release beneath Damar, vertical stretching due to seismic release is occurring at several times this at rates approaching 10^{-14} s^{-1}.

In summary, seismic moment release rates suggest the Damar Zone slab is deforming at rates of 10^{-15} to 10^{-14} s^{-1} in the 100–200 km depth range. The deformation involves vertical stretching accompanied by across slab thinning and, generally strike parallel stretching. A localized zone beneath the island of Damar is characterized by horizontal constriction and the highest rates of vertical stretching. Vertical stretching rates drop rapidly east of ∼129°E.

5 IMPLICATIONS FOR BANDA SLAB DYNAMICS

Variation in both intensity and character of intermediate depth seismicity points to significant complexity in the seismogenic deformation field in the Banda slab. As noted in a number of previous studies, the most striking aspect is the variability in intermediate depth activity between the Wetar and Damar Zones. The seismic moment data summarized here for the first time indicates vertical stretching in the Damar Zone at rates of up to $\sim 10^{-14}$ s^{-1}, greater in the west than the east, lending strong credence to the idea that the slab is rupturing in this region, propagating eastwards in the depth range 100–200 km and widening a slab-window beneath Wetar (Fig. 11). In this context, it is relevant to note that a mean vertical stretching rate of 2×10^{-14} s^{-1} over a depth range of 100 km, produces the differential displacement of ∼60 km Myr^{-1}, more or less

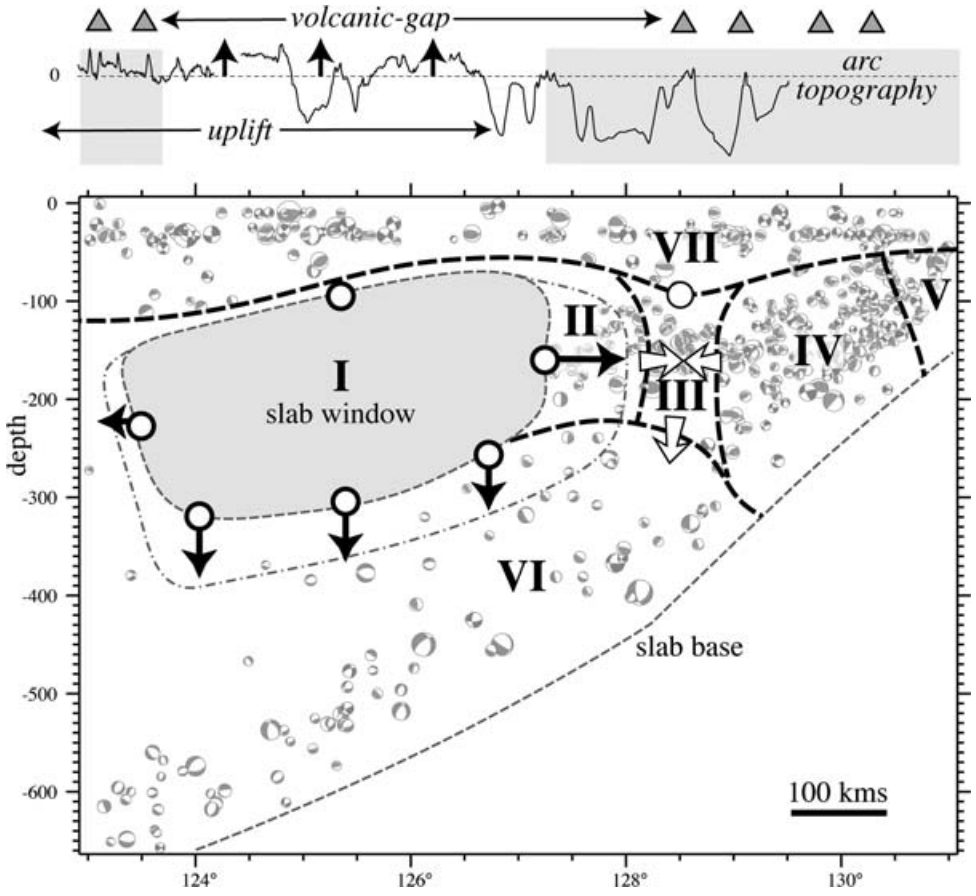

Figure 11. Schematic synthesis of inferred slab dynamics in the Banda Sea based on the analysis of the CMT moment distribution presented in this paper. Variations in the moment tensor release allow subdivision of the slab and overlying lithosphere in the region 124–131°E into a number of distinct domains: (I) a domain characterized by an intermediate depth seismic gap in the Wetar Zone, (II) the western segment of the Damar Zone, characterized by down dip *T*-axes, *P*-axes at a high angle to the slab trend and a mild flattening strain field (Fig. 6a), (III) the centralwest segment of the Damar Zone characterized by down dip *T*-axes, *P*-axes in the plane of the slab and a constrictional strain field (Fig. 6b), (IV) the centraleast segment of the Damar Zone characterized by slab-normal *P*-axes trends and oblique *T*-axes (Fig. 6c), (V) an eastern segment in which *P*-axes lie in the plane of the slab as noted by Cardwell & Isacks (1978), (VI) the lithospheric domain characterized by shallow *P*-axes aligned with plate convergence (see also Fig. 5) and (VII) the domain of deep seismicity characterized by near vertical *P*-axes indicative of downdip compression. The constrictional strain field that characterizes domain III (white arrows) is postulated to reflect stress concentration imparted from the deeper, now semi-detached segment slab beneath domain I, which may also cause the anomalously deep bathymetry of the overlying arc. In domain II the slab maybe more or less completely decoupled, with the slab rupture front propagating rapidly eastwards (as suggested by the narrow dash–dotted line). Black arrows show relative inferred velocities of the boundaries of domain I, with the lower boundary assumed to be sinking at ∼60–70 km Myr^{-1}, consistent with complete decoupling from the Australian plate, and the opening of a ∼200 km deep slab window in domain I since 3 Ma coincident with the intermediate depth seismic gap.

matching the absolute speed of the Australian plate (Genrich *et al*. 1996). Assuming that the deeper parts of the slab system are sinking at long term rates governed by Australian plate motion, then the Banda slab must be close to complete decoupling in the western segment of the Damar Zone across the depth interval 100–200 km. Indeed, with the possibility that seismic deformation accounts for no more than ∼50 per cent of the total strain then this segment of the slab could already be effectively fully decoupled. Such a notion is consistent with the absence of volcanism west of Damar as well as with the occurrence of great earthquakes such as the 1963 M_w 8.3 event, the moment of which requires that it ruptured the entire seismogenic core of slab over several hundred kilometres (Osada & Abe 1981). As the seismic core of the slab thins deformation should accelerate, and thus the strain rates deduced form moment release suggest the characteristic timescale for slab rupture in the Damar Zone is no more than $\sim 10^6$ yr.

As first noted by Cardwell & Isacks (1978) and subsequently by McCaffrey *et al.* (1985) the abundance of slab parallel *P*-axes trends in the Banda slab is unusual. Beyond about 130.5°E (domain V in Fig. 11), the slab parallel *P*-axes have been related to the unusually tight folding of the eastern most part of the Banda slab (Cardwell & Isacks 1978). The analysis presented here shows there is also a narrower zone of slab-parallel *P*-axes beneath the island of Damar in the region of most rapid vertical stretching (domain III in Fig. 11). An apparent small discontinuity in the trend of intermediate depth seismicity allows the possibility of minor folding of the slab in the vicinity of Damar (Fig. 7) that might help explain the in-plane *P*-axis trends (see also Das 2004). However, probably more important is the fact that the zone of anomalous *P*-axis trends occurs in a relative sharp gradient in the vertical moment release rate as reflected most prominently in the reduced moment release estimates presented here. As such, the zone of anomalous *P*-axis trends may simply reflect in-plane horizontal shortening induced by the differential vertical stretching rates to either side. However, the moment release rates imply that this region is also unusual in that it is experiencing horizontal constriction. An important consequence of

partial slab rupture is that negative buoyancy from the ruptured segments must lead to stress concentration in the region ahead of the rupture front (Fig. 11). The hypothesis advanced here is that the zone of constriction near Damar reflects stress concentration ahead of an eastward propagating slab rupture front. The notion that the rupturing slab segment beneath Damar is more highly stressed than other parts of the system is consistent with the unusually low bathymetry of this segment arc, evident in the >2 km deep ocean gateways (Fig. 3). This bathymetric anomaly points to a significant negative dynamic topography that would be expected to accompany increased stress transfer through the slab (see further discussion below).

Assuming that the Wetar slab-window has grown to its present width since the cessation of volcanism at about 3 Ma, then the time-averaged rate of lateral propagation rate must be $\sim$130 km Myr^{-1}. Presumably, some of the widening of the slab window is occurring at the western end of the Wetar Zone, beneath Pantar (McCaffrey *et al.* 1985). However, the intermediate depth seismic moment release rate beneath the Flores Zone is much lower than beneath the Damar Zone (Fig. 3), and the westward propagation rate into the Flores Zone is likely much less than its eastward propagation rate into the Damar Zone (Fig. 11). It seems likely therefore that the slab window front is propagating eastward into the Damar Zone at rates of $\sim$100 km Myr^{-1}, consistent with the seismogenic stretching rates in the 100-km long western part of the Damar Zone.

As noted earlier the differences in topographic character of the arc between the Wetar and Damar Zones are striking and arguably relate to dynamic topographic effects mediated by the changing pattern of stress transmission through the rupturing slab. Two consequences of this rupturing should be evident in the evolving surface topographic field. First, as stress transmission from the deeper, negatively buoyant parts of the slab is reduced, the surface above ruptured segments should be experience uplift (Chatelain *et al.* 1992). Second, increased stress transmission through the slab ahead of the rupture front should induce subsidence above the intact segment of the slab, as well as enhancing seismicity. While the Wetar Zone is demonstrably uplifting at a regional average of about 0.5 mm yr^{-1}, there is no evidence pertaining to a corresponding active subsidence above the Damar Zone apart from the indirect evidence implied by the remarkably low elevation of the arc here. Clearly such evidence would provide a profound test of a propagating slab rupture, and would hold important clues as to the dynamics of stress transmission through the slab, as well as the evolution of the Indonesian seaways that have been postulated as so important to late Neogene climate change in the continents bounding the Indian Ocean (Cane & Molnar 2001). For example, if subsidence of the Damar Zone was antithetic to the uplift of the Wetar Zone at around 0.5 mm yr^{-1}, then the ocean gateways to the east of Wetar will have deepened on average by more than 50 per cent over the last 1 Myr. Since these are by far the largest gateways through the Indonesian arc system, such a scenario may be expected to have significant oceanographic and climatic ramifications (Cane & Molnar 2001).

ACKNOWLEDGMENTS

Shamita Das kindly provided her catalogue of relocated Indonesian earthquakes. Reviews by Meghan Miller and an anonymous reviewer helped sharpen the focus of this work. This work was funded by ARC Discovery grant DP0556133.

REFERENCES

Abbott, M.J. & Chamalaun, F.H., 1981. Geochronology of some Banda Arc volcanics, *Special Publication – Geological Research and Development Centre, Republic of Indonesia,* **2,** 253–271.

Audley-Charles, M.G., 2004. Ocean trench blocked and obliterated by Banda forearc collision with Australian proximal continental slope, *Tectonophysics,* **389,** 65–79.

Cane, M.A. & Molnar, P., 2001. Closing of the Indonesian seaway as a precursor to east African aridification around 3–4 million years ago, *Nature,* **411,** 57–162.

Cardwell, R. & Isacks, B., 1978. Geometry of subducted lithosphere beneath the Banda Sea in eastern Indonesia from seismicity and fault-plane solutions, *J. geophys. Res.,* 2825–2838.

Chappell, J. & Veeh, H.H., 1978. Late quaternary tectonic movements and sea-level changes at Timor and Atauro Island, *Geol. Soc. Am. Bull.,* **89,** 356–368.

Chatelain, J.-L., Molnar, P., Prévot, R. & Isaaks, B., 1992. Detachment of part of the down going slab and uplift of the New Hebrides (Vanuatau) Islands, *Geophys. Res. Lett.,* **19,** 1507–1510.

Das, S., 2004. Seismicity gaps and the shape of the seismic zone in the Banda Sea Region from relocated hypocenters, *J. geophys. Res.,* 109, doi:10.1029/2004JB003192.

Davies, J.H. & von Blackenburg, F., 1995. Slab breakoff: a model of lithosphere detachment and its test in the magmatism and deformation of collisional orogens, *Earth planet. Sci. Lett.,* **129,** 85–102.

Elburg, M.A., van Bergen, M.J. & Foden, J.D., 2004. Subducted upper and lower continental crust contributes to magmatism in the collision sector of the Sunda-Banda arc, Indonesia, *Geology,* **32,** 41–44.

Engdahl, E.R. & Villaseñor, A., 2002. Global seismicity: 1900–1999, in *International Handbook of Earthquake and Engineering Seismology, Part A,* Chapter 41, pp. 665–690, eds W.H.K. Lee, H. Kanamori, P.C. Jennings & C. Kisslinger, Academic Press, Amsterdam.

Gasparon, M., Hilton, D.R. & Varne, R., 1994. Crustal contamination processes traced by helium isotopes: examples from the Sunda arc, Indonesia, *Earth planet. Sci. Lett.,* **126,** 15–22.

Genrich, J.F.Y.B., McCaffrey, R., Calais, E., Stevens, C.W. & Subayra, C., 1996. Accretion of the southern Banda arc to the Australian plate margin determined by Global Positioning System measurements, *Tectonics,* **15,** 288–295.

Gerya, T., Yuen, D.A. & Maresch, W.V., 2004. Thermo-mechanical modelling of slab detachment, *Earth planet. Sci. Lett.,* **226,** 101–116.

Hanks, T.C. & Kanamori, H., 1979. A moment-magnitude scale, *J. geophys. Res.,* **84,** 2348–2350.

Hantoro, W.S. *et al.*, 1994. Quaternary uplifted coral reef terraces on Alor Island, East Indonesia, *Coral reefs,* **13,** 215–223.

Hilton, D.R., Hoogewerff, J.A., van Bergen, M.J. & Hammerschmidt, K., 1992. Mapping magma sources in the east Sunda-Banda arcs, Indonesia: constraints from helium isotopes, *Geochim. Cosmochim. Acta,* **56,** 851–859.

Hilton, D.R., Hammerschmidt, K., Loock, G. & Friedrichsen, H., 1993. Helium and argon isotope systematics of the central Lau Basin and Valu Fa Ridge: evidence of crust/mantle interactions in a back-arc basin, *Geochim. Cosmochim. Acta,* **57,** 2819–2841.

Houston, H., 1993. The non-double-couple component of deep earthquakes and the width of the seimogenic zone, *Geophys. Res. Lett.,* **20,** 1687–1690.

Johnston, A.C., Coppersmith, K.J., Kanter, L.R. & Cornell, C.A., 1994. The earthquakes of stable continental regions, *Electric Power Research Institute Publication TR–102261–V1,* Palo Alto, California.

Kanamori, H., 1997. The energy release of great earthquakes, *J. geophys. Res.,* **82,** 2981–2987.

Kostrov, B.V., 1974. Seismic moment and energy of earthquakes, and seismic flow of rocks, *Izvestia Acad. Sci. USSR Phys. Solid Earth* **1,** 23–40.

McCaffrey, R., 1989a. Seismological constraints and speculations on Banda arc tectonics, *Netherlands J. Sea Res.,* **24,** 141–152.

McCaffrey, R., 1989b. Seismological constraints and speculations on Banda Arc tectonics, *Netherlands J. Sea Res.,* **24,** 141–152.

McCaffrey, R. & Abers, G.A., 1991. Orogeny in arc–continent collision: the Banda Arc and western New Guinea, *Geology,* **19,** 563–566.

McCaffrey, R., Molnar, P., Roecker, S.W. & Joyodirwiryo, Y.S., 1985. Microearthquake seismicity and fault plane solutions related to arc continent collision in the eastern Sunda Arc, Indonesia, *J. geophys. Res.,* **90,** 4511–4545.

Merritts, D., Eby, R., Harris, R., Edwards, R.L. & Chang, H., 1998. Variable rates of Late Quaternary surface uplift along the Banda Arc-Australian plate collision zone, eastern Indonesia, *Geol. Soc., Lond., Special Publications,* **146,** 213–224.

Meulen, M.J.v.d., Meulenkamp, J.E. & Wortel, M.J.R., 1998. *Earth planet. Sci. Lett.,* **154,** 203–219.

Milsom, J., 2001. Subduction in eastern Indonesia: how many slabs? *Tectonophysics,* **338,** 167–178.

Milsom, J., 2005. The Vrancea seismic zone and its analogue in the Banda Arc, eastern Indonesia, *Tectonophysics,* **410,** 325–336.

Nothard, S., Haines, J., Jackson, J. & Holt, B., 1996. Distributed deformation in the subducting lithopshere at Tonga, *Geophysical. J. Int.,* **127,** 328–338.

Okal, E.A. & Reymond, D., 2003. The mechanism of great Banda Sea earthquake of 1 February 1938: applying the method of preliminary determination of focal mechanism to a historical event, *Earth planet. Sci. Lett.,* **216,** 1–15.

Osada, M. & Abe, K., 1981. Mechanism and tectonic implications of the great Banda Sea earthquake of November 4, 1963, *Phys. Earth planet. Inter.,* **25,** 129–139.

Pirazzoli, P.A., Radtke, U., Hantoro, W.S., Jouannic, C., Hoang, C.T., Causse, C. & Best, M.B., 1991. Quaternary raised coral-reef terraces on Sumba Island, Indonesia, *Science,* **252,** 1834–1836.

Replumaz, A., Karason, H., Van Der Hilst, R.D., Besse, J. & Tapponnier, P., 2004. 4-D evolution of SE Asia's mantle from geological reconstructions and seismic tomography, *Earth planet. Sci. Lett.,* **221,** 103–115.

Schoffel, H.-J. & Das, S., 1999. Fine details of the Wadati-Benioff zone under Indonesia and its geodynamic implications, *J. geophys. Res.,* **104,** B6.

Spakman, W., 1990. Tomographic images of the upper mantle below central Europe and the Mediterranean, *Terra Nova,* **2,** 542–553.

Widiyantoro, S. & Van Der Hilst, R.D., 1997. Mantle structure beneath Indonesia inferred from high-resolution tomographic imaging, *Geophys. J. Int.,* **130,** 167–182.

Wong, A., Ton, S.Y.M. & Wortel, M.J.R., 1997. Slab detachment in continental collision zones: an analysis of controlling parameters, *Geophys. Res. Lett.,* **24,** 2095–2098.

Yoshioka, S. & Wortel, M.J.R., 1995. Three-dimensional modeling of detachment of subducted lithosphere, *J. geophys. Res.,* **100,** 20 223–20 244.